emerald PUBLISHING

International Journal of Numerical Methods for He
Flui

The effects of GDL anisotropic transport properties on the PEFC performance

Journal:	*International Journal of Numerical Methods for Heat and Fluid Flow*
Manuscript ID	HFF-05-2022-0284.R1
Manuscript Type:	Research Article
Keywords:	Polymer electrolyte fuel cells, Gas diffusion layers, Numerical model, Anisotropic transport properties

Abstract

Purpose – This paper aims to numerically investigate the impact of gas diffusion layer (GDL) anisotropic transport properties on the overall and local performance of polymer electrolyte fuel cells (PEFCs).

Design/methodology/approach – A three-dimensional numerical model of a polymer electrolyte fuel cell with a single straight channel has been developed to investigate the sensitivity of the fuel cell performance to the GDL anisotropic transport properties – gas permeability, diffusivity, thermal conductivity, and electrical conductivity. Realistic experimentally estimated GDL transport properties were incorporated into the developed PEFC model, and a parametric study was performed to show the effect of these properties on fuel cell performance and the distribution of the key variables of current density and oxygen concentration within the cathode GDL.

Findings – The results showed that the anisotropy of the GDL must be captured to avoid overestimation/underestimation of the performance of the modelled fuel cell. The results also showed that the fuel cell performance and the distributions of current density and oxygen mass fraction within the cathode GDL are highly sensitive to the through-plane electrical conductivity of the GDL and, to a lesser extent, the through-plane diffusivity, and the thermal conductivity of the GDL. The fuel cell performance is almost insensitive to the gas permeability of the GDL.

Practical implications – The current study improves the understanding of the importance of the GDL anisotropy in the modelling of fuel cells and provides useful insights on improving the efficiency of the fuel cells.

Originality/value – Realistic experimentally estimated GDL transport properties has been incorporated into the PEFC model for the first time, allowing for more accurate prediction of the PEFC performance.

1. Introduction

The gas diffusion layer (GDL) of the polymer electrolyte fuel cell (PEFC) is made up of solid (carbon, binder, and PTFE) and void phases. It is a crucially important component for the PEFC as it is responsible for the transport of gas reactants, heat and electrons between the flow-field plates and the catalyst layers, and provision of mechanical support to the delicate catalyst layers (Carcadea et al., 2007; El-Kharouf and Pollet, 2012). It is evident that limited transfer rate of gas reactants to the catalyst layers results in a decreased overall PEFC performance (Hassan et al., 2011; Ismail et al., 2016; Chen et al., 2020). On the other hand, high availability of reactant gases in the catalyst reaction sites does not only improves fuel cell performance but also reduces the amount of precious platinum catalyst required for the electrochemical reactions in the cell, thus making the PEFC more efficient and cost-effective (Gostick et al., 2006). To this end, the GDL should possess high mass transport properties (i.e., gas diffusivity and permeability) to quickly supply enough reactant gases to the catalyst layers and at the same time effectively remove excess water generated at the cathode catalyst layer. Equally the GDL should demonstrate high electrical conductivity to minimise ohmic losses and high thermal conductivity to dissipate/keep heat generated within the membrane electrode assembly (MEA) and subsequently prevent the dry-out of the membrane electrolyte or water flooding (Chen et al., 2020).

The conventional GDLs are made from carbon fibres which are preferentially oriented in the in-plane direction, thus resulting in anisotropic transport properties (Ismail et al., 2012). To this end, there have been several experimental and numerical studies on investigating the

anisotropic nature of the GDL and estimating its transport properties in different principal directions. Zamel et al. (2012) developed a 3-D reconstruction model of a carbon paper GDL to numerically estimate the effective electrical conductivity, at different values of porosity, for both through -plane and in-plane directions. They found the in-plane electrical conductivity to be higher than that in the through-plane direction by about 25% for high GDL porosity values between 0.7 to 0.9 and by about 44% for low porosity values between 0.4 to 0.6. They also proposed mathematical correlations to determine the effective electrical conductivity for the carbon fibre paper GDL and found the tortuosity factor to be 3.4 in the through-plane direction while for the in-plane it was reported to be 1.7. Zamel et al. (2010) numerically estimated the effective thermal conductivity of untreated carbon fibre paper GDL and found the thermal conductivity to be higher in the in-plane as compared to that of the through-plane by a factor of about 2. Veyret and Tsotridis (2010) developed a 3-D numerical model to estimate the effective thermal conductivity of the GDL. They reported that the anisotropic ratio for the GDL thermal conductivity (i.e., the ratio between the in-plane and the through- plane thermal conductivity) increases with increasing GDL porosity. Kramer et al. (2008) applied electrochemical impedance spectroscopy (EIS) to measure the effective diffusivity in the in-plane and through-plane directions as a function of the compression of the GDL paper and found that the in-plane effective diffusivity decreased from 0.6 to 0.2, at a porosity of 50%. While that of the through-plane direction decreased from 0.3 to 0.1. Fluckiger et al. (2008), using the electrochemical diffusimetry method initially developed by Kramer et al. (2008), measured the in-plane and through-plane diffusivities for three different carbon fibre paper materials. They investigated the effect of the binder structure and the Teflon treatment on the anisotropy and the effective diffusivity of the different GDL samples. They showed that an improved through-plane diffusivity is essential for high limiting current densities. Also, they reported that the ratio of the in-plane diffusivity to the through-plane diffusivity depends on

the orientation of the carbon fibres, the properties of the binders, the PTFE treatment as well as the GDL compression. Ramousse et al. (2008) theoretically and experimentally estimated the thermal conductivity of Quintech, and SGL carbon felts used as GDL in PEFCs. They reported the effective thermal conductivity of the carbon felts to be an order of magnitude lower than those of pure carbon papers measured in most literature. Ismail et al. (2010,2011) experimentally measured the through-plane and in-plane gas permeability for multiple coated and uncoated SGL GDLs. They found that the through-plane gas permeability of the coated GDLs is one order of magnitude lower than the corresponding in-plane gas permeability. In another work, Ismail et al. (2010) measured the in-plane and through-plane conductivity of uncoated and coated SGL GDL samples and found that the in-plane conductivity (when incorporating the contact resistance between the GDL and the bipolar plate) is two orders of magnitude higher than the through-plane conductivity and this is mainly due to the preferential alignment of the carbon fibres in the in-plane directions. Gostick et al. (2006) measured the gas permeability in three principal directions for several carbon fibre GDL substrates including SGL and Toray GDLs. They also measured the in-plane permeability of the GDL samples as a function of compression. They reported that the GDL samples with the most highly aligned fibres displayed the highest anisotropy, and their through-plane and in-plane permeability values could differ by a factor of 2. Becker et al. (2009) combined both experimental and numerical approaches to characterise the anisotropic transport properties of a Toray TGP-H-060 carbon paper. They reported the in-plane diffusivity to be twice that of the through-plane. They also found the in-plane permeability to be four times higher than the through-plane permeability. Likewise, the in-plane electrical conductivity was found to be an order of magnitude higher than that in the through-plane direction. Using periodic surface modelling, Didari et al. (2014) numerically characterised the gas permeability and the relative diffusivity for a Toray GDL. They reported the through-plane and the in-plane permeabilities to be 6.8 ×

$10^{-12}\mathrm{m}^2$ and $1.19 \times 10^{-11}\mathrm{m}^2$, respectively. While the through-plane and the in-plane relative diffusivities of the GDL was found to be 0.42 and 0.67, respectively. Gostick (2013) developed a 3D pore network model of the GDL to numerically characterise the diffusivity of Toray carbon GDL and found the through-plane diffusivity to be 0.21 while that of the in-plane direction was reported to be 0.45. James et al. (2012) used X-ray computed tomography of the GDL to numerically estimate transport properties of an SGL carbon substrate: 30BA. They showed that the effective electrical conductivity and diffusivity in the in-plane directions are four times larger than those in the through-plane direction. Nam and Kaviany (2003) developed a numerical model to estimate the effective diffusivity of carbon fibre GDL as a function of the porosity of the GDL and water saturation. They showed that the fibre alignment in the lateral direction, where there is no pore blockage, results in a higher in-plane effective diffusivity. Also, at low porosities (less than 0.45), the through-plane diffusivity was found to be larger than that in the in-plane direction.

Clearly not capturing the anisotropic nature of the GDL in the PEFC models would negatively impact the accuracy of the predictions of the PEFC models. The literature shows that there have been some attempts to investigate the impact of the anisotropic GDL on the performance of the modelled PEFCs. Pharaoh et al. (2006) investigated the effect of the anisotropic diffusivity and electrical conductivity on the performance of the modelled PEFC cathode. They showed that treating the electrodes as isotropic porous media yields significantly different current density predictions than anisotropic treatments. Using a 2-D single phase numerical PEFC, Bapat and Thynell (2008) investigated the effects of the anisotropic thermal conductivity and the thermal contact conductance on temperature distribution in the PEFC. They reported that though an increase in the in-plane thermal conductivity of the GDL resulted in smaller temperature gradients, the improvement in the heat transport is limited by the thermal contact resistance between the GDL and the bipolar plate. Pasaogullari et al. (2004) developed

a 2-D, non-isothermal, two-phase cathode side PEFC model to investigate the effect of the GDL anisotropy on the coupled heat and mass transfer within the cathode of the PEFC. They showed that the maximum temperature difference in the GDL is a strong function of the of the GDL anisotropy. Also, they reported that relatively high in-plane thermal conductivity values result in significantly different liquid water saturation distributions. Hyunchul (2009) developed a 3-D, two -phase PEFC model to study the effects of GDL anisotropic transport properties on the PEFC performance as well as on the heat and water transport in the cell. The author reported a significant variation of the PEFC temperature along the through-plane direction when the in-plane thermal conductivity is an order of magnitude higher than the through-plane thermal conductivity. Alhazmi et al. (2013) numerically investigated the effect of the GDL anisotropic thermal conductivity at three different PEFC operating temperatures, using a 3-D multiphase model of the PEFC. They reported a greater sensitivity of the temperature gradients within the PEFC to the in-plane thermal conductivity of the GDL as opposed to that of the through -plane direction. They also reported an increase in the power density of the PEFC when the in-plane and through-plane thermal conductivities are increased. Xing et al. (2015) studied the effect of GDL anisotropy on the transport of species, electric charge, heat, and liquid water in PEFCs operated at various loads, using a non-isothermal multi-phase flow numerical model of the PEFC. They reported that the anisotropic gas diffusivity does not influence the PEFC cell performance at low current densities, but it does at higher current densities. Their results showed negligible influence of the anisotropic gas permeability and thermal conductivity on the PEFC performance. Yoshimune et al. (2022) experimentally measured the through-plane diffusivity for Toray carbon paper GDL, TGP-H-060, using infrared absorption carbon dioxide sensor. They found the through-plane diffusivity of the GDL sample to be 0.36 ± 0.02 at a temperature of 25℃. Taş and Elden (2020) experimentally measured the through-plane and in-plane electrical conductivities of SGL34BA and SGL34BC

gas diffusion layers. They investigated the effects of the PEFC operating temperature, the relative humidity, and the clamping pressure on the anisotropic electrical conductivities of the tested gas diffusion materials. They reported no significant change in the in-plane electrical conductivity, of both the SGL34BA and SGL34BC GDL samples, with increasing PEFC operating temperature and clamping pressure. However, there was a significant change in the in-plane electrical conductivity for the measured GDL samples under different relative humidities. Taş and Elden (2022) numerically developed a three-dimensional PEFC model in which they integrated their previously experimentally measured values of the anisotropic electrical conductivities for the above-mentioned gas diffusion layers. In their model, they investigated the effects of the PEFC operating temperature and the relative humidity on the anisotropic electrical conductivities of the GDL samples. They reported an increase in the output current densities in the in-plane direction with an increase in the temperature. For the through-plane directional component, they reported a maximum value of current density in the region of the GDL lying underneath the ribs of the bipolar plates. Zhang et al. (2017) developed a three-dimensional multiphase PEFC model to investigate the channel and gas diffusion layer flows in the PEM fuel cell. They investigated the effect of the GDL anisotropic effective electrical conductivity, gas diffusivity and permeability (but not the thermal conductivity) on the performance of the modelled PEFC. They reported the oxygen mass fraction distribution to be overpredicted for the case with isotropic GDL transport properties. Wang et al. (2022) developed a three-dimensional multiphase PEFC model with a through-plane and in-plane synergetic gradient porosity distribution in the cathode gas diffusion layer. They reported that a higher porosity within the region of the GDL lying close to the flow channel improves the transport of the gas reactants and the liquid water removal from the PEFC; this results in a uniform distribution of oxygen and current density within the cathode GDL. Yu et al. (2022) also developed a three-dimensional, non-isothermal and two-phase PEFC model incorporating

the difference in porosities of the region of the GDL under the rib and that under the gas flow channel. They investigated the effects of the GDL anisotropic transport properties on the current density distribution within the PEFC, temperature distribution, liquid water, and gas reactant concentrations. In addition, they reported that there is a lower current density distribution at the region of the GDL lying under the gas channel when the cell is operated at lower cell voltages. Ismail et al. (2012) developed a 3-D PEFC model of an in-house built PEFC to study the effects of the GDL anisotropic gas permeability and electrical conductivity on the performance of the PEFC. They found that the PEFC performance to be almost insensitive to the GDL anisotropic permeability and highly sensitive to the GDL anisotropic electrical conductivity. Li et al. (2017) developed a 3-D, two-phase, non-isothermal model of the PEFC in which they investigated the effects of GDL anisotropic gas permeability, gas diffusivity thermal conductivity and electrical conductivity on PEFC performance. They demonstrated that the temperature of the anisotropic case is more uniform and lower than that of the isotropic case owing to the relatively high in-plane thermal conductivity at high current densities. They also reported severe liquid water saturation in the isotropic GDL case model as compared to that of the anisotropic case.

Notably, in all the above studies, there have been no three-dimensional numerical PEFC models that incorporated the experimentally measured multidimensional values of each of the gas diffusivity, the gas permeability, the thermal conductivity, and the electrical conductivity of the GDLs. Therefore, to improve predictions, we have built a three-dimensional PEFC model which accounts for the anisotropic nature of the GDLs though employing experimentally measured values of the above key transport properties. After validating the model, we have performed a parametric study by realistically increasing/decreasing the base experimentally-estimated value of each of the above-mentioned transport properties. This is done to investigate the impact of not capturing the anisotropy for each of the above-mentioned transport properties

on the performance of the modelled PEM fuel cell and the distribution of the key variables of current density and oxygen concentration, and subsequently obtain insights on how to improve the fuel cell efficiency.

2. Model description and transport equations

This section details the conservation equations that govern the transport of the physical quantities and their source terms as well as the electrochemical reactions which occur within the PEM fuel cell. The PEFC model developed in this study is based on the PEFC model of Berning et al. (2002).

2.1. Model assumptions

The following assumptions are made to simplify the PEFC model:

- Steady-state operation.
- Laminar and incompressible flow.
- Membrane is impermeable to the reactant gases.
- Uniform compression on all components of the fuel cell.
- Water exists in vapour phase only to isolate the impact of water saturation and solely focus on the impact of the GDL anisotropy.

2.2. Model geometry

The computational domain of the PEFC model consists of cathode and anode bipolar plates (or current collectors), cathode and anode flow channels, cathode and anode catalyst layers and the membrane electrolyte. The computational domain is, to save computational time, limited to a portion incorporating cathode and anode straight gas flow channels. Further, due to symmetry,

only half channel width is considered; see Figure 1. The geometrical, operational, and physical parameters are presented in Table 1.

[Figure 1]

2.3. Transport equations

The following equations govern the transport of the physical quantities in all components of the modelled PEFC (Gostick et al., 2006; Ismail et al., 2012; Bruggeman, 1935; Pharaoh et al, 2006; Alhazmi et al., 2013; Li et al., 2017; Zawodzinski et al., 1993):

Mass transport equation

$$\nabla \cdot (\varepsilon \rho \vec{u}) = 0 \tag{1}$$

where ρ is the gas mixture fluid density, ε is the porosity and $\vec{u}$ is the fluid velocity vector.

Momentum transport equation

$$\nabla \cdot (\varepsilon \rho \vec{u}\vec{u}) = -\varepsilon \nabla P + \nabla \cdot (\mu \nabla \varepsilon \vec{u}) + \frac{\varepsilon^2 \mu \vec{u}}{K} \tag{2}$$

where P is the pressure of gas mixtures, μ is the dynamic viscosity of the fluid and K is the permeability of the porous medium.

Species transport equation

$$\nabla \cdot (\varepsilon \rho \vec{u} Y_k) = \nabla \cdot (\rho D_{kj}^{eff} \nabla Y_k) + S_k \tag{3}$$

where Y_k is the mass fraction of species k and D_{kj}^{eff} is the effective binary diffusivity of species j into k. D_{kj}^{eff} is calculated using the Bruggeman's correlation as follows (Bruggeman, 1935):

$$D_{kj}^{eff} = \varepsilon^{\tau} D_{kj} \tag{4}$$

where τ is the tortuosity of the porous medium and D_{jk} is bulk binary diffusivity of species k into j. S_k is the source term that represents either consumption/production of species k (H_2, O_2 or H_2O) and is given as follows (Ismail et al., 2012):

$$S_{H_2} = -\frac{i_a a_a}{2F} M_{H_2} \tag{5}$$

$$S_{O_2} = -\frac{i_c a_c}{4F} M_{O_2} \tag{6}$$

$$S_{H_2O} = \frac{i_c a_c}{2F} M_{H_2O} \tag{7}$$

where i_a and i_c are the anodic and cathodic local current density respectively, a_a and a_c are the anodic and cathodic specific surface areas respectively, F is Faraday's constant (96485 C/mol) and M_{H_2}, M_{O_2} and M_{H_2O} are the molecular weights for hydrogen, oxygen and water, respectively.

Energy transport equation

$$\nabla \cdot (\rho c_p \vec{u} T) = \nabla \cdot (k_{eff} \nabla T) + S_e \tag{8}$$

where T is the temperature, c_p is the specific heat capacity of the gas mixtures, k_{eff} is the effective thermal conductivity. S_e is the heat source term and takes one of the following forms in each fuel cell component (Li et al., 2017):

$$S_e = \begin{cases} i_s^2/\sigma_s \; for \; anode \; and \; cathode \; GDLs \\ R_a\left[\eta_a - \frac{T\Delta S_a}{2F}\right] + \frac{i_s^2}{\sigma_s} + \frac{i_m^2}{\sigma_m} \; for \; anode \; catalyst \; layer \\ R_c\left[-\eta_c - \frac{T\Delta S_c}{2F}\right] + \frac{i_s^2}{\sigma_s} + \frac{i_m^2}{\sigma_m} \; for \; cathode \; catalyst \; layer \end{cases} \tag{9}$$

where R_a and R_c are the anode and cathode exchange current densities, i_s and i_m are the solid phase and membrane phase current densities, σ_s and σ_m are the electrical and ionic conductivities of the solid and membrane phases respectively, and η_a and η_c are the anodic and

cathodic overpotential, ΔS_a and ΔS_c are the reaction entropies at anode and cathode catalyst layers respectively.

Charge transport equations

Two potential equations for the electronic and ionic conduction are solved. The equations are expressed as follows:

$$\nabla \cdot (\sigma_s \nabla \phi_s) = S_{\phi,s} \tag{10}$$

$$\nabla \cdot (\sigma_m \nabla \phi_m) = S_{\phi,m} \tag{11}$$

where ϕ_s and ϕ_m are the electrical (solid phase) and ionic (membrane phase) potentials respectively. $S_{\phi,s}$ and $S_{\phi,m}$ are the solid-phase potential and membrane-phase potential respectively and are given as follows (Alhazmi et al., 2013):

$$S_{\phi,s} = \begin{cases} j_a \; at \; the \; anode \; CL \\ -j_c \; at \; the \; cathode \; CL \end{cases} \tag{12}$$

$$S_{\phi,m} = \begin{cases} -j_a \; at \; the \; anode \; CL \\ j_c \; at \; the \; cathode \; CL \end{cases} \tag{13}$$

where j_a and j_c are the volumetric exchange current density (A/m³) at the anode and cathode catalyst layers respectively and are obtained using Butler-Volmer equations (Zawodzinski et al., 1993):

$$j_a = i_a^{ref} a_a \left(\frac{c_{H_2}}{c_{H_2}^{ref}}\right)^{0.5} \left[exp\left(\frac{\alpha_{a,a}F}{RT}\eta_{act,a}\right) - exp\left(\frac{\alpha_{a,c}F}{RT}\eta_{act,a}\right)\right] \tag{14}$$

$$j_c = i_c^{ref} a_c \left(\frac{c_{O_2}}{c_{O_2}^{ref}}\right) \left[exp\left(\frac{\alpha_{c,a}F}{RT}\eta_{act,c}\right) - exp\left(\frac{\alpha_{c,c}F}{RT}\eta_{act,c}\right)\right] \tag{15}$$

where i_a^{ref} and i_c^{ref} are the reference anodic and cathodic exchange current density respectively, $\alpha_{a,a}$ and $\alpha_{a,c}$ are respectively the anode and cathode transfer coefficients for the electrochemical

reactions in the anode catalyst layer, $\alpha_{c,a}$ and $\alpha_{c,c}$ are respectively the anode and cathode transfer coefficients in the cathode catalyst layer, $c_{H_2}^{ref}$ and $c_{O_2}^{ref}$ are the reference hydrogen and oxygen concentrations respectively, F is the Faraday's constant and R is the universal gas constant. $\eta_{act,a}$ and $\eta_{act,c}$ are the anodic and cathodic overpotential and are given as follows:

$$\eta_{act,a} = \phi_s - \phi_m \tag{16}$$

$$\eta_{act,c} = \phi_s - \phi_m - E_0 \tag{17}$$

where E_0 is the reference potential of the electrodes and is equal to zero for the anode, while for the cathode it is equal to the equilibrium cell potential (E_r) (Gostick et al., 2006; Pharaoh et al., 2006):

$$E_r = 1.482 - 0.000845T + 0.0000431T\ln\left(P_{H_2}P_{O_2}^{0.5}\right) \tag{18}$$

The membrane ionic conductivity, σ_m, is estimated using an empirical correlation developed by Springer et al. (1991):

$$\phi_m = (0.005139\lambda - 0.00326)\exp\left[1268\left(\frac{1}{303} - \frac{1}{T}\right)\right] \tag{19}$$

where λ is the membrane water content which is empirically correlated by Zawodzinski et al.(1993):

$$\lambda = \begin{cases} 1.409 + 11.26ac - 18.77ac^2 + 16.21ac^3, & 0 < ac \leq 1 \\ 10.11 + 2.944(ac - 1), & 1 < ac \leq 3 \\ 16.8, & ac > 3 \end{cases} \tag{20}$$

where ac is the water activity and is given as (Ismail et al., 2012):

$$ac = \frac{P_v}{P_s} \tag{21}$$

where P_v is the partial pressure of water vapour and P_s is the pressure of saturated water vapor which is given by (Ismail et al., 2012):

$$\log(P_s) = -2.1794 + 0.02953(\mathrm{T} - 273.15) - 9.1837 \times 10^{-5}(\mathrm{T} - 273.15)^2 + 1.4454 \times 10^{-7}(\mathrm{T} - 273.$$

(22)

2.4. Boundary conditions and numerical procedure

Velocity inlet boundary conditions are specified for the anode and cathode gas flow channels. The operating temperature (353K) and the species mass fractions are specified at the flow channel inlets. The fluid inlet velocity is defined as a function of a typical operating current density (i_{op}) which is in this case 500 mA/cm², the active area of the fuel cell (A_{act}), the channel cross-sectional area (A_{ch}), and the stoichiometric ratio (ξ) of the reactant gas which was set as 2 for both hydrogen and oxygen gases. Therefore, the anodic and the cathodic inlet velocities are given as follows (Berning et al., 2002):

$$u_a = \xi_a \frac{i_{op}}{2F} A_{act} \frac{1}{X_{H_2} P_a} \frac{RT}{A_{ch}} \quad (23)$$

$$u_c = \xi_c \frac{i_{op}}{4F} A_{act} \frac{1}{X_{O_2} P_c} \frac{RT}{A_{ch}} \quad (24)$$

Zero-flux boundary conditions are specified for all wall boundaries, except for the anode and cathode terminals (i.e., the top surfaces of the current collectors). The pressure outlet boundary conditions are specified at the outlet of the gas flow channels. Potentiostatic boundary conditions are specified for the anode and cathode current collector terminals of the cell, respectively, with the electrical potential for the anode set to zero (ground voltage) and that of the cathode set to the cell operating voltage (V_{cell}). A constant operating temperature of 353K is set for both the anode and cathode terminals. The equations governing the transport of mass, heat, and charge in the PEFC model and the coupled boundary conditions were solved iteratively, using the commercial software ANSYS FLUENT. The Semi-implicit Method for Pressure Linked Equations (SIMPLE) algorithm is employed for the pressure–velocity coupling with the second-order upwind discretization scheme for the conservation of

momentum, species, energy, and charge equations. The model was found to give mesh-independent solution with a mesh of about 1.4 million cells; doubling this number result in a variation of less than 0.3% in the key performance indicator which is, in this case, the average current density at 0.55 V. The distribution of the mesh is shown in Figure 2.

[Figure 2 and Table 1]

3. Results and discussion

The modelled PEFC was simulated for different cell voltages and the polarisation curve was then generated. Figure 3 shows that the modelling data results are in good agreement with the experimental data extracted from Ticianelli et al. (1998). However, the model slightly under-predicts the performance of the fuel cell at lower cell voltages. This is most likely to be due to the fact that the physics of the liquid water (which at higher current densities increases the water content of the membrane electrolyte phase to be of the order of 20s rather than 10s and subsequently improves the ionic conductivity (Duan et al., 2012)) has not been captured in this single-phase model.

[Figure 3]

3.1. Anisotropic GDL versus isotropic GDLs

Experimentally measured and realistic GDL anisotropic transport properties (gas permeability, gas diffusivity, thermal conductivity, and electrical conductivity) of the PEFC obtained from the literature, as shown in Table 2, are inputted into the PEFC model. We strived to ensure that for all the experimentally estimated transport properties to be of the same GDL material (i.e., SGL 10BA) (Ismail et al., 2012; Alhazmi et al., 2013). However, for the gas diffusibility values, we used those of Kramer et al. (2008) and this was due to the unavailability of the corresponding values for SGL 10BA; nonetheless, this should not affect the general trends presented and the overall conclusions. The polarisation curve of the modelled PEFC with the

anisotropic GDL transport properties as well as the local distribution of key variables (the current density and oxygen mass fraction) within its cathode GDL are compared with those for the modelled PEFC model having isotropic GDL transport properties; see Figure 4. The isotropic transport properties are assumed to be the same as those of the through-plane direction for Case 2 and the same as those for the in-plane direction for Case 3; see Table 2.

[Table 2]

Figure 4a shows that the model over-predicts the fuel cell performance if the GDL transport properties are assumed to be isotropic and having the same values as those of the in-plane direction; for example, at 0.4 V, the current density is over-predicted by about 38%. On the other hand, the model under-predicts the fuel cell performance if the GDL transport properties are assumed to be isotropic and having the same values as those of the through-plane direction. However, the model is less sensitive the "isotropic through-plane" assumption (Case 2) compared to the "isotropic in-plane" assumption (Case 3). Namely, at 0.4 V, the current density is under-predicted by about 25% when switching from Case 1 to Case 2. Figure 4b compares the current density distribution at 0.55 V within the cathode GDL, halfway along the length of the channel of the PEFC, for both isotropic (through-plane and in-plane) and anisotropic cases. The local current density distribution in all cases have similar trends. For all three cases, the local current density is minimum at the section of the GDL which lies under the midpoint of the channel and increases steadily towards the interface between the collector rib and the gas channel where it peaks and then drops at the region beneath the current collector rib (this is more evident for Cases 1 and 3). This is attributed to the fact that the interface between the flow channel and the current collector is where the supply of oxygen and the transport of electrons are both optimised (the transport of oxygen to the catalyst layer is a minimum beneath the mid-point of the rib and the transport of electrons is a minimum beneath the mid-point of

the flow channel). The local current density is significantly higher in Case 3 compared to Cases 1 and 2 and this evidently is due to the significantly higher in plane electrical conductivity which is assumed to be having the same value as the experimentally estimated in-plane conductivity shown in Table 2 (i.e., 4000 S/m). Case 2 shows that the current density saturates beneath the rib of the current collector, and this is due to lack of high in-plane conduction; this should be compared with Case 1 where the high in-plane conduction (4000 S/m) is responsible for "spreading" the current density more uniformly within the GDL. As expected, Fig. 4c shows that, for all cases, the concentration of oxygen (in the form of oxygen mass fraction) is maximum under the midpoint of the flow channel and minimum under the mid-point of the rib of the current collector. Note that Case 3 demonstrates lower oxygen concentration within the GDL, and this is due to the consumption of higher amount of oxygen at the cathode catalysts layer compared to Cases 1 and 2; this is induced by the higher overall electrical conduction of Case 3.

[Figure 4]

3.2. Parametric study

As this study is aimed at investigating the sensitivity of the PEFC performance to the anisotropic key transport properties of the GDL (the gas permeability, mass diffusivity, thermal conductivity, and electrical conductivity), a parametric study of the individual transport properties of the GDL was examined.

3.2.1. Anisotropic gas permeability

Table 3 shows the 5 computational cases considered to investigate the impact of the gas permeability. Case 1 is the case in which the experimentally estimated gas permeability in through-plane and in-plane directions were fed into the model. In Cases 2 and 3, the experimentally measured through-plane gas permeability is kept constant and the

experimentally measured in-plane gas permeability is decreased and increased by an order of magnitude respectively. Likewise, in Cases 4 and 5, the experimentally measured in-plane gas permeability is kept constant and the experimentally measured through-plane gas permeability is decreased and increased by an order of magnitude. The results of the simulated cases are represented in Figure 5. Figure 5a shows that the linear profiles of the current density within the cathode GDL almost overlap each other; the same can be observed about the profiles of the oxygen concentration within the cathode GDL at 0.55 V. Further, the average current density at 0.55 V for all the cases shows a very minimal variation between the cases (the variation lies in the fourth decimal place). This signifies the very minimal impact of the GDL gas permeability on the performance of the fuel cell. As mentioned in prior works of Ismail et al. (2012); Zamel et al. (2012) observed that the main mode of transport within the GDL is diffusion, not convection.

[Table 3 and Figure 5]

3.2.2. Anisotropic effective diffusivity

The effective diffusivity within the GDL is often estimated using Bruggeman's correlation which is ε^{τ} in Equation (4). The ratio between the effective diffusivity and the bulk diffusivity (which is Bruggeman's correlation in our case) is called the diffusibility. As with gas permeability, the experimentally estimated diffusibility in Case 1 has been realistically decreased and increased in through-plane and in-plane directions; see Table 4. This table shows that the average current density at 0.55 V changes very slightly with the changes in the in-plane diffusibility (compare Cases 1, 2 and 3). However, the average current density becomes more sensitive to changes in the through-plane diffusibility (compare Cases 1, 4 and 5); for example, the current density, for a given in-plane diffusibility of 0.5, increases by around 5% when the through-plane diffusibility increases from 0.1 to 0.5. Figure 6 shows the current density, and

the oxygen concentration profiles within the cathode GDL. As with the average current density, Figure 6a shows that, compared to the base case (Case 1), the local current density is more sensitive to the through-plane diffusibility (Cases 4 and 5) than the in-plane diffusibility (Cases 2 and 3). This is since the through-plane direction is the direction through which the reactant gas (oxygen in this case) transport from the flow channel to the catalyst layer where it is consumed, thus completing the reaction, and generating the electrical current. For example, the mean local current density (averaged over the distance considered within the cathode GDL) increases by around 11% when the GDL diffusibility increases from 0.1 to 0.5.

Figure 6b shows that the oxygen mass fraction within the cathode under the flow channel is the lowest for Case 5 where the through-plane diffusibility is the largest, signifying higher amount of oxygen is consumed compared to other cases; this in line with the current density profiles shown in Figure 6a which demonstrates that the current density is in general the highest for Case 5. On the other hand, the oxygen concentration under the rib is the lowest for Case 2. This is because the in-plane diffusibility is the lowest for this case and as such the transport of oxygen from the regions below the flow channel to the regions below the rib is most hindered compared to other cases. On a related note, Cases 1, 2 and 3 do not show any remarkable difference in the distribution of oxygen in the region of the GDL below the channel. This shows that the in-plane diffusibility has no major impact on the oxygen distribution within this region. The in-plane diffusibility begins to dominate the distribution of oxygen as we approach the interface between the channel and the collector rib.

[Table 4 and Figure 6]

3.2.3. Anisotropic thermal conductivity

As with the GDL gas permeability and diffusibility, Table 5 shows five cases in which Case 1 is the case with the experimentally estimated values for the through- and in-plane thermal

conductivity and the other 4 cases are the cases where the through-plane and the in-plane thermal conductivity values are realistically changed to investigate the sensitivity the fuel cell performance to the anisotropic GDL thermal conductivity. Overall, the impact of the GDL thermal conductivity on the fuel cell performance is, compared to electrical conductivity or even gas diffusivity, rather small; the difference in the average current density at 0.55 V between the best case (Case 4) and the worst case (Case 5) is just about 13.4 mA/cm². The reason that Case 4 shows the best performance is that the significantly reduced through-plane thermal conductivity (i.e., 0.01 W/m□K) decreases heat dissipation rate, increases cell temperature, and subsequently increases the rate of reaction (as evidenced from the Butler-Volmer equation shown in Equations (14) and (15) and the membrane conductivity (as evidenced from the Springer's model shown in Equation (19). In general, any decrease in either the in-plane thermal conductivity (compare Cases 1, 2 and 3) or the through-plane conductivity (compare Cases 1, 4 and 5) results in a slight improvement to the fuel performance. The distribution of current density within the cathode GDL (Figure 7a) are in line with the average current density results shown in Table 6; marginal gain are obtained with decreasing either the in-plane or the through-plane GDL thermal conductivities. Evidently, better cell performance means higher oxygen consumption rate and subsequently less oxygen concentration within the GDL and that is why Case 4 demonstrates the least oxygen mass fraction within the cathode GDL (Figure 7b).

[Table 5 and Figure 7]

3.2.4. Anisotropic electrical conductivity

Table 6 shows 5 computation cases where the first case (Case 1) is the case with the experimentally estimated values for the through- and in-plane electrical conductivity and the other 4 cases are the cases where the through-plane and the in-plane electrical conductivity values are realistically changed to investigate the sensitivity the fuel cell performance to the

anisotropic GDL electrical conductivity. Further, Figure 8 displays the distribution of current density and oxygen concentration within the cathode GDL at 0.55 V. The first observation that could be extracted from Table 6 and Figure 8 is that the fuel cell performance and the distributions of current density and oxygen concentration are much more sensitive to the GDL electrical conductivity than the other transport properties. The reason behind this is that the electrical conductivity is associated with the ohmic losses which are the main potential losses for typically operating cell voltages (0.5 - 0.6 V). The second observation is that the fuel cell performance is significantly more sensitive to the through-plane electrical conductivity (compare Cases 1, 4 and 5) than to the in-plane electrical conductivity (compare Cases 1, 2 and 3). To illustrate, the average current density at 0.55 V increases by more than 50% when increasing the through-plane GDL conductivity from 24 S/m (Case 4) to 96 S/m (Case 5). On the other hand, the average current density increases by less than 5% when increasing the in-plane GDL electrical conductivity from 2000 S/m (Case 2) to 8000 S/m (Case 3). This is mainly since the shortest (and the least resistive) pathway for the electrons to reach the catalyst layers (where they combine with oxygen and protons to produce water) is across the thickness of the GDL, not along the plane of the GDL.

Figure 8a shows that, for a given through-plane electrical conductivity, as the in-plane electrical conductivity increases (Cases 1, 2 and 3), the linear distribution of current density within the GDL expectedly becomes more uniform due to decreased in-plane electrical resistance. Further, in accordance with the average current density results at 0.5 V, it is evident that local current density is much more sensitive to the through-plane electrical conductivity (compare Cases 1, 4 and 5) than to the in-plane electrical conductivity (compare Cases 1, 2 and 3). This observation is also applicable to the distribution of oxygen distribution; the largest gap is between Case 4 and Case 5 where the through-plane electrical conductivity are 24 and 48 S/m

respectively. As expected, the lowest oxygen concentration within the GDL is demonstrated by Case 5 where the oxygen consumption rate is the maximum for this case.

[Table 6 and Figure 8]

5. Conclusions

A three-dimensional straight channel PEFC model has been developed. The main purpose of this study is to investigate the sensitivity of the fuel cell performance and the distributions of the key variables within the GDL (current density and oxygen concentration) to the anisotropy in the key transport properties of the GDL: gas permeability, gas diffusivity, thermal conductivity, and electrical conductivity. The key findings and observations are as follows:

- The anisotropic nature of the conventionally used GDLs need to be captured in the PEFC models. Overlooking this GDL's attribute leads to either significant overestimation (if the in-plane values of the transport properties are considered) or underestimation (if the through-plane values of the transport properties are considered) of the modelled fuel cell current density by up to 50% at typical cell voltages.
- The fuel cell performance and the distribution of current density and oxygen concentration within the GDL are, compared to other transport properties, highly sensitive to the electrical conductivity of the GDL, particularly in the through-plane direction. Quadrupling the through-plane GDL electrical conductivity increases the average current density of the fuel cell at 0.55 V by more than 50%.
- On the other hand, the fuel cell performance, and the distributions of the above key variables within the GDL are almost insensitive to the through-plane or in-plane gas permeability of the GDL as the main mode of transport within the GDL is diffusion.

- The fuel cell performance is moderately sensitive to both the gas diffusivity (represented by the diffusibility in this study) and, to a lesser extent, the thermal conductivity of the GDL. This observation is more evident with the through-plane diffusibility and the thermal conductivity than with in-plane diffusibility or the thermal conductivity of the GDL. This is mainly since the mass and heat transport to/from the catalyst layer from/to the flow channel/rib is in the through-plane direction. Notably, the fuel cell performance improves with decreasing the GDL through-plane thermal conductivity as it lowers heats dissipation and increases the reaction rate at the cathode catalyst layer.

- It is recommended that in the design and manufacture of the fibre GDLs, the carbon fibre needs to be more oriented in the through-plane direction as against the conventional in-plane direction as the GDL transport properties in that direction will improve the performance of the PEFC.

Based on the findings of the study, it is recommended to design GDLs with superior through-plane electrical conductivity and, to a lesser extent, through-plane diffusibility and thermal conductivity. This could be achieved by having more carbon fibres oriented in the through-plane direction.

Nomenclature

a	*Specific surface area,* m^{-1}
A_{ch}	*Channel cross-sectional area,* m^2
c	*Concentration,* mol/m^3
D	*Diffusivity,* m^2/s
E_0	*Reference potential, V*
E_r	*Equilibrium potential, V*
F	*Faraday constant, C/mol*
i	*Current density,* A/m^2
i_0	*Exchange current density,* A/m^2

i_{op}	*Operating current density,* A/m^2
j	*Volumetric transfer current,* A/m^3
K	*Permeability,* m^2
M	*Molecular weight, kg/mol*
P	*Pressure, Pa*
R	*Universal gas constant,* $J/mol \cdot K$
R_a	*Anode exchange current density*
R_c	*Cathode exchange current density*
S	*Source term in conservation equations*
T	*Cell operating temperature, K*
$\vec{u}$	*Velocity vector, m/s*
Y	*Mass fraction*
ΔS	*Entropy*

Greek symbols

ρ	*Density,* kg/m^3
μ	*Dynamic viscosity,* $Pa \cdot s$
σ	*Electrical/ionic conductivity, S/m*
β	*Inertial coefficient*
η	*Over-potential, V*
ε	*Porosity*
ϕ	*Potential, V*
κ	*Thermal conductivity,* $W/m \cdot K$
$\propto$	*Transfer coefficient*
ξ	*Stoichiometric ratio*

Subscripts

a	*Anode*
act	*Activation*
c	*Cathode*
e	*Energy*
k,j	*Species*
m	*Membrane phase*
s	*Solid phase*
sat	*Water saturation*
v	*Water vapor*
$_{=}$	*In-plane*
$_{\perp}$	*Through-plane*

Superscripts

eff	*Effective*
ref	*Reference value*

Abbreviations

GDL	*Gas diffusion layer*
MEA	*Membrane electrode assembly*
PEFC	*Proton exchange membrane fuel cell*
PTFE	*Polytetraflouroethylene*

Chemical symbols

H_2	*Hydrogen molecule*
H_2O	*Water molecule*
O_2	*Oxygen molecule*

References

Alhazmi, N., Ingham, D. B., Ismail, M.S., Hughes, K. J., Ma, L. and Pourkashanian, M. (2013), "Effect of the anisotropic thermal conductivity of GDL on the performance of PEM fuel cells", International Journal of Hydrogen Energy, Vol.38, pp. 603-611.

Alhazmi, N., Ismail, M.S., Ingham, D. B., Hughes, K. J., Ma, L. and Pourkashanian, M. (2013), "The in-plane thermal conductivity and the contact resistance of the components of the membrane electrode assembly in proton exchange membrane fuel cells", Journal of Power Sources, Vol.241, pp. 136-145.

Bapat, C. and Thynell, S.T. (2008), "Effect of anisotropic thermal conductivity of the GDL and current collector rib width on two-phase transport in a PEM fuel cell", Journal of Power Sources, Vol.179 No.1, pp. 240-251.

Becker, J., Fluckiger, R., Reum, M., Buchi, F.N., Marone, F. and Stampanoni, M. (2009), "Determination of Material Properties of Gas Diffusion Layers: Experiments and Simulations Using Phase Contrast Tomographic Microscopy", Journal of the Electrochemical Society, Vol.156 No.10, pp. 1175- 1181.

Berning, T., Lu, D.M. and Djilali, N. (2002), "Three-dimensional computational analysis of transport phenomena in a PEM fuel cell", Journal of Power Sources, Vol. 106 No. 1-2, pp. 284–294.

Bruggeman, D.A.G. (1935), "Calculation of various physics constants in heterogeneous substances I dielectricity constants and conductivity of mixed bodies from isotropic substances", Annalen der Physik (Leipzig), Vol. 24, pp. 636-664.

Carcadea, E., Ene, H., Ingham, D.B., Lazar, R., Ma, L., Pourkashanian, M. and Stefanescu, I. (2007), "A computational fluid dynamics analysis of a PEM fuel cell system for power generation", International Journal of Numerical Methods for Heat and Fluid Flow, Vol. 17 No. 3, pp. 302-312.

Chen, Z., Ingham, D., Ismail, M. , Ma, L., Hughes, K.J. and Pourkashanian, M. (2020), "Effects of hydrogen relative humidity on the performance of an air-breathing PEM fuel cell: A numerical study", International Journal of Numerical Methods for Heat and Fluid Flow, Vol. 30 Nos 4, pp. 2077-2097.

Didari, S., Asadi, A., Wang, Y., and Harris, T.A.L. (2014), "Modelling of composite fibrous porous diffusion media", International Journal of Hydrogen Energy, Vol.39, pp. 9375-9386.

Duan, Q., Wang, H., and Benziger, J. (2012), "Transport of liquid water through Nafion membranes", Journal of Membrane Science, Vol.392-393, pp. 88-94.

El-Kharouf, A. and Pollet, B. G. (2012), "Gas Diffusion Media and their Degradation", Polymer Electrolyte Fuel Cell Degradation. DOI: 10.1016/B978-012-386936-4.10004-1.

Flückiger, R., Freunberger, S. A., Kramer, D., Wokaun, A., Scherer, G. G. and Büchi, F. N. (2008), "Anisotropic, effective diffusivity of porous gas diffusion layer materials for PEFC", Electrochim Acta, Vol.54 No.2, pp. 551-559.

Gostick, J.T., Fowler, M. W., Pritzker, M. D., Ioannidis, M. A. and Behra, L. M. (2006), "In-plane and through-plane gas permeability of carbon fibre electrode backing layers", Journal of Power Sources, Vol.162 No.1, pp. 228-238.

Gostick, J. T. (2013), "Random pore network modeling of fibrous PEMFC gas diffusion media using Voronoi and Delaunay tessellations", Journal of the Electrochemical Society, Vol.160, pp. 731- 743.

Hasan, A.B.M., Wahab, M.A. and Guo, S.M. (2011), "CFD analysis of a PEM fuel cell for liquid dispersion at the interface of GDL-GFC", International Journal of Numerical Methods for Heat and Fluid Flow, Vol. 21 No. 7, pp. 810-821.

Hyunchul, J. (2009), "Investigation of the effects of the anisotropy of gas-diffusion layers on heat and water transport in polymer electrolyte fuel cells", Journal of Power Sources, Vol.191, pp. 259-268.

Ismail, M. S., Damjanovic, T., Ingham, D. B., Ma, L. and Pourkashanian, M. (2010), "Effect of polytetrafluoroethylene-treatment and microporous layer-coating on the in-plane permeability of gas diffusion layers used in proton exchange membrane fuel cells", Journal of Power Sources, Vol. 195, pp. 6619 – 6628.

Ismail, M. S., Damjanovic, T., Ingham, D. B., Pourkashanian, M. and Westwood A. (2010),"Effect of polytetrafluoroethylene-treatment and microporous layer-coating on the electrical conductivity of gas diffusion layers used in proton exchange membrane fuel cells", Journal of Power Sources, Vol. 195 No.9, pp. 2700-2708.

Ismail, M., Borman D., Damjanovic, T., Ingham, D.. and Pourkashanian, M. (2011), "On the through-plane permeability of microporous layer-coated gas diffusion layers used in proton exchange membrane fuel cells", International Journal of Hydrogen Energy, Vol.36 No.16, pp. 10392-10402.

Ismail, M. S., Hughes, K. J., Ingham, D. B., Ma, L. and Pourkashanian, M. (2012), "Effects of anisotropic permeability and electrical conductivity of gas diffusion layers on the

performance of proton exchange membrane fuel cells", Applied Energy, Vol. 95, pp. 50 – 63.

Ismail, M., Ingham, D., Hughes, K.J., Ma, L. and Pourkashanian, M. (2016), "The effects of shape on the performance of cathode catalyst agglomerates in polymer electrolyte fuel cells", International Journal of Numerical Methods for Heat and Fluid Flow, Vol. 26 Nos 3/4, pp. 1145-1156.

James, J. P., Choi, H.W.and Pharaoh, J. G. (2012), "X-ray computed tomography reconstruction and analysis of polymer electrolyte membrane fuel cell porous transport layers", International Journal of Hydrogen Energy, Vol.37, pp. 18216-18230.

Kramer, D., Freunberger, S. A., Flückiger, R., Schneider, I. A., Wokaun, A., Büchi, F. N. et al. (2008), "Electrochemical diffusimetry of fuel cell gas diffusion layers", Journal of Electroanal Chemistry, Vol.612 No. 1, pp. 63-77.

Li, S., Yuan, J., Andersson, M., Xie, G. and Sundén, B. (2017), "Influence of anisotropic gas diffusion layers on transport phenomena in a proton exchange membrane fuel cell", International Journal of Energy Research, Vol 41, pp.2034- 2050.

Nam, J. H. and Kaviany, M. (2003), "Effective diffusivity and water-saturation distribution in single-and two-layer PEMFC diffusion medium", International Journal of Heat and Mass Transfer, Vol.46, pp. 4595-4611.

Pasaogullari, U., Mukherjee, P.P., Wang, C. Y. and Chen, K. S. (2004), "Anisotropic Heat and Water Transport in a PEFC Cathode Gas Diffusion Layer", Journal of the Electrochemical Society, Vol.151 No.3, pp. A399-A406.

Pharaoh, J. G., Karan, K. and Sun, W. (2006), "On effective transport coefficients in PEM fuel cell electrodes: Anisotropy of the porous transport layers", Journal of Power Sources, Vol.161 No.1, pp. 214-224.

Ramousse, J., Didierjean, S., Lottin, O. and Maillet, D. (2008), "Estimation of the effective thermal conductivity of carbon felts used as PEMFC Gas Diffusion Layers", International Journal of Thermal Sciences, Vol. 47 No.1, pp. 1-6.

Springer, T. E., Zawodzinski, T. A. and Gottesfeld, S. (1991), "Polymer electrolyte fuel-cell model", Journal of the Electrochemical Society, Vol 138 pp.2334–42.

Taş, M. and Elden, G. (2020), "An Experimental Investigation of the Effects of Operating Conditions on Anisotropic Electrical Conductivity in a PEM Fuel Cell", Fuel Cells, Vol.20 No. 5, pp. 531-539.

Taş, M. and Elden, G. (2022), "Three-dimensional and anisotropic numerical analysis of a PEM fuel cell", International Journal of Hydrogen Energy, Vol. 47, pp. 19758-19771.

Ticianelli, E. A., Derouin, C. R., Redondo, A. and Srinivasan, S. (1998), "Methods to Advance Technology of Proton-Exchange Membrane Fuel-Cells", Journal of the Electrochemical Society, Vol 135 No.9, pp.2209-2214.

Veyret, D. and Tsotridis, G. (2010), "Numerical determination of the effective thermal conductivity of fibrous materials: application to proton exchange membrane fuel cell gas diffusion layers", Journal of Power Sources, Vol. 195, pp. 1302-1307.

Wang, Y., Wang, X., Qin, Y., Zhang L. and Wang, Y. (2022), "Three-dimensional numerical study of a cathode gas diffusion layer with a through/in plane synergetic gradient porosity distribution for PEM fuel cells", International Journal of Heat and Mass Transfer, Vol 188 No. 122661, pp.1-15.

Xing, L., Das, P. K., Song, X. G., Mamlouk, M. and Scott, K. (2015), "Numerical analysis of the optimum membrane/ionomer water content of PEMFCs: the interaction of Nafion ionomer content and cathode relative humidity", Applied Energy, Vol 138, pp.242–257.

Yoshimune, W., Kato, S., Inagaki, M. and Yamaguchi, S. (2022), "A simple method to measure through-plane effective gas diffusivity of a gas diffusion layer for polymer electrolyte fuel cells", International Journal of Heat and Mass Transfer, Vol 191 No. 122887, pp.1-7.

Yu, R. J., Guo H., and Ye, F. (2022), "Study on transmission coefficients anisotropy of gas diffusion layer in a proton exchange membrane fuel cell", Electrochimica Acta, Vol. 414, pp. 1-18.

Zamel, N., Xianguo, L., Shen, J., Becker, J. and Wiegmann, A. (2010), "Estimating effective thermal conductivity in carbon paper diffusion media", Chemical Engineering Science, Vol.65 No.13, pp. 3994-4006.

Zamel, N., Li, X. and Shen, J. (2012), "Numerical estimation of the effective electrical conductivity in carbon paper diffusion media", Applied Energy, Vol. 93, pp. 39-44.

Zawodzinski, T. A., Springer, T. E., Uribe, F. and Gottesfeld, S. (1993), "Characterisation of polymer electrolytes for fuel cell applications", Solid State Ionics, Vol 60 pp.199–211.

Zhang, G., Fan, L., Sun, J. and Jiao, K. (2017), "A 3D model of PEMFC considering detailed multiphase flow and anisotropic transport properties", International Journal of Heat and Mass Transfer, Vol 115, pp.714-724.

Table 1 Geometrical and physical properties for the base case of the PEFC model. Sources: Berning et al. (2002); Ismail et al. (2012); Zawodzinski et al. (1993).

Property	Value
Channel length	5×10^{-2} m
Channel height	1.0×10^{-3} m
Channel width	1.0×10^{-3} m
Land area width	1.0×10^{-3} m
GDL thickness	0.26×10^{-3} m
Catalyst layer thickness	1.0×10^{-5} m
Membrane thickness	0.23×10^{-3} m
Operating temperature	353 K
Gauge pressure at anode	5 atm
Gauge pressure at cathode	3 atm
Relative humidity of inlet gases	100%
Oxygen/nitrogen molar ratio in air	0.21/0.79
Catalyst layer porosity	0.4
GDL porosity	0.7
GDL permeability	4.97×10^{-13} m^2
Reference hydrogen concentration, $c_{H_2}^{ref}$	40 mol/m^3
Reference oxygen concentration, $c_{O_2}^{ref}$	40 mol/ m^3
Electrical conductivity of solid phase	6000 S/m
Ionic conductivity of the membrane	0.6 S/m
Catalyst layer permeability	1×10^{-13} m^2
Membrane permeability	1.8×10^{-18} m^2
Thermal conductivity of GDLs	75 W/(m-K)
Thermal conductivity of catalyst layers	75 W/(m-K)
Thermal conductivity of Bipolar plates	75 W/(m-K)
Thermal conductivity of the membrane	0.67 W/(m-K)
Faraday's constant	96485 C/mol
Universal gas constant	8.314 J/(mol-K)
Active area	11.56×10^{-4} m^2
Anode inlet mass fraction of hydrogen	0.37
Anode inlet mass fraction of water	0.63
Cathode inlet mass fraction of oxygen	0.21
Cathode inlet mass fraction of water	0.103
Cathode inlet mass fraction of nitrogen	0.69

Anode concentration exponents	0.5
Cathode concentration exponents	1
Anode reference exchange current density, $i_{0,a}^{ref}$	6000 A/m²
Cathode reference exchange current density, $i_{0,c}^{ref}$	0.0044 A/m²
Transfer coefficients for anode reaction	0.5
Transfer coefficients for cathode reaction	1
Anode specific surface area, a_a	1.0×10^7 m^{-1}
Cathode specific surface area, a_c	1.0×10^7 m^{-1}

Table 2 Key GDL transport properties in through-plane and in-plane directions.

	Case 1		Case 2	Case 3
Transport properties	**Through-plane**	**In-plane**	**Isotropic (Through-plane)**	**Isotropic (In-plane)**
Permeability (m^2) Source: Ismail et al. (2012)	4.97×10^{-13}	1.87×10^{-12}	4.97×10^{-13}	1.87×10^{-12}
Diffusibility (m^2/s). Source: Kramer et al. (2008)	0.3	0.5	0.3	0.5
Thermal Conductivity (W/m-K) Source: Li et al. (2017)	1.7	21	1.7	21
Electrical Conductivity (S/m) Source: Ismail et al. (2012)	48	4000	48	4000

Table 3 Computation cases for the GDL gas permeability investigation. Source: Ismail et al. (2012).

Case Number	Permeability (m^2)		Average Current density (A/cm^2) at 0.55 V
	Through-plane, $K_{\perp}$	In-plane, $K_{=}$	
1	4.97×10^{-13}	1.87×10^{-12}	0.5016
2	4.97×10^{-13}	1.87×10^{-13}	0.5015
3	4.97×10^{-13}	1.87×10^{-11}	0.5017
4	4.97×10^{-14}	1.87×10^{-12}	0.5016
5	4.97×10^{-12}	1.87×10^{-12}	0.5017

Table 4 Computation cases for the GDL gas diffusivity investigation. Source: Kramer et al. (2008).

Case Number	Diffusibility		Average Current density (A/cm²) at 0.55 V
	Through-plane, f $(\varepsilon)_{\perp}$	In-plane, f $(\varepsilon)_{=}$	
1	0.3	0.5	0.5115
2	0.3	0.3	0.5109
3	0.3	0.7	0.5119
4	0.1	0.5	0.4932
5	0.5	0.5	0.5155

Table 5 Computation cases for the GDL thermal conductivity investigation. Source: Alhazmi et al. (2013).

Case Number	Thermal Conductivity (W/m.K)		Average Current density (A/cm²) at 0.55 V
	Through-plane	In-plane	
1	0.1	10	0.5029
2	0.1	1	0.5054
3	0.1	100	0.5017
4	0.01	10	0.5089
5	1	10	0.4955

Table 6 Computation cases for the GDL electrical conductivity investigation. Source: Ismail et al. (2012).

Case Number	Electrical Conductivity (S/m)		Average Current density (A/cm²) at 0.55 V
	Through-plane	In-plane	
1	48	4000	0.493
2	48	2000	0.480
3	48	8000	0.503
4	24	4000	0.386
5	96	4000	0.580

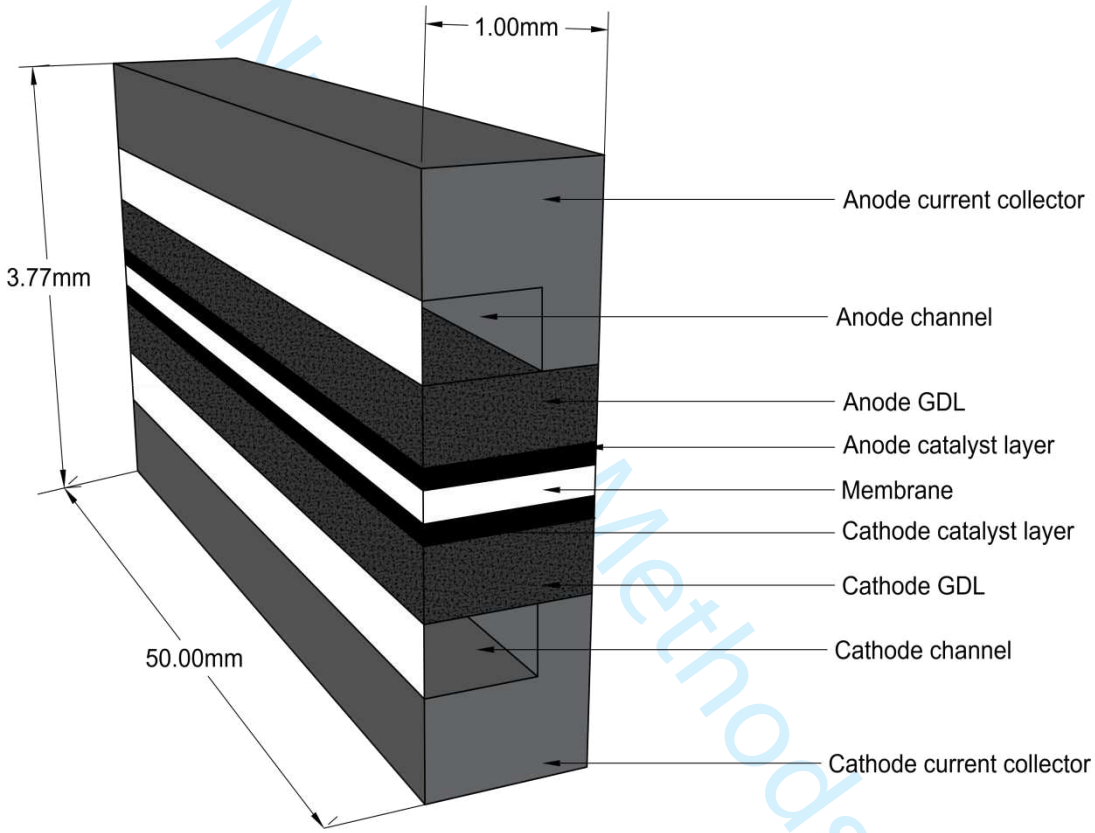

Figure 1 A Schematic of the computational domain.

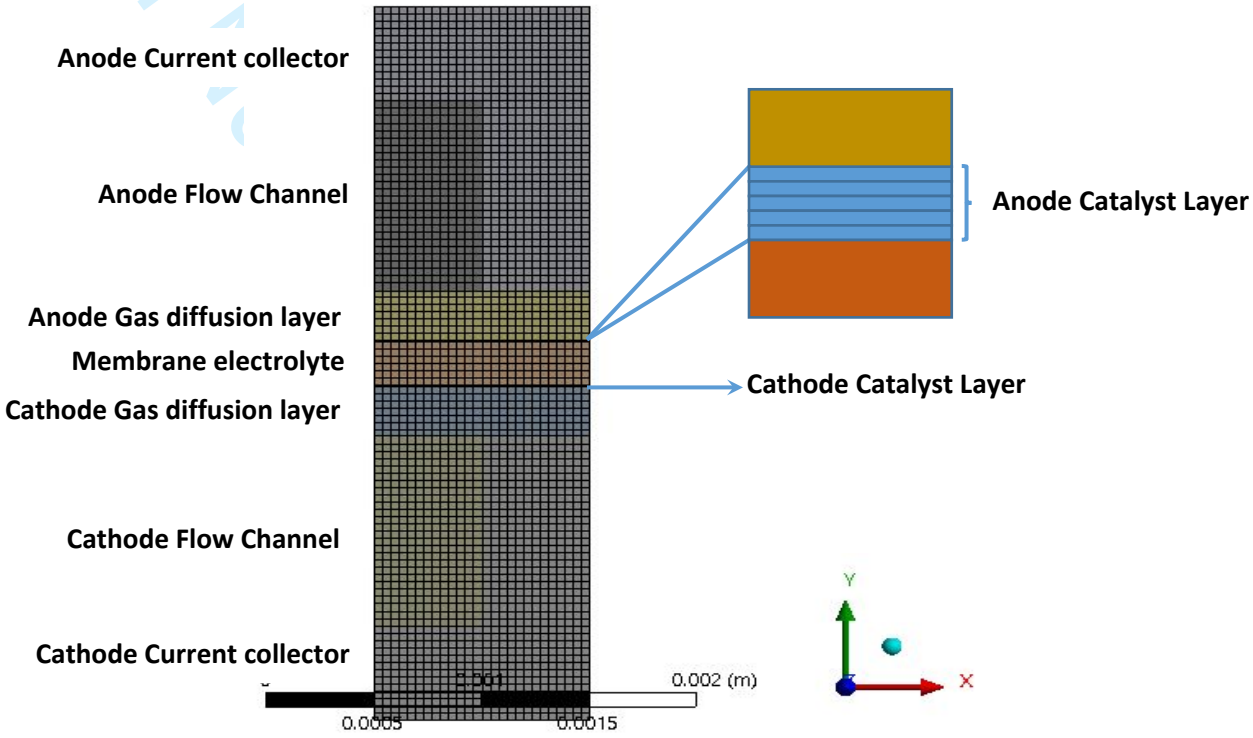

Figure 2 The mesh profile of the front view of the geometry. Note that (i) the anode catalyst layer has been zoomed in to show the mesh across the catalyst layer and (ii) the number of elements in the z-direction is 350.

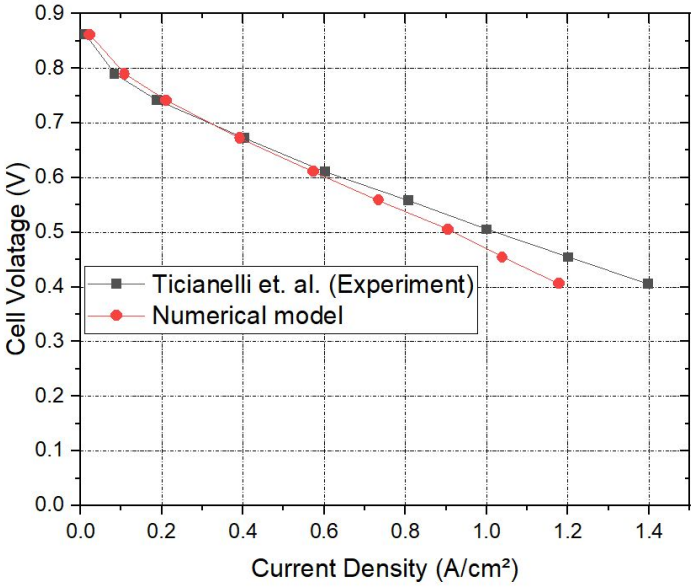

Figure 3 The polarization curve generated from the numerical model as compared to the experimental polarization curve taken from Ticianelli et al. (1998).

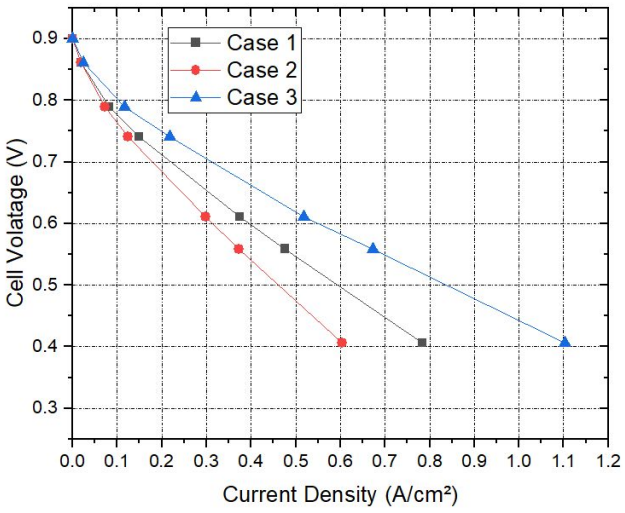

(a)

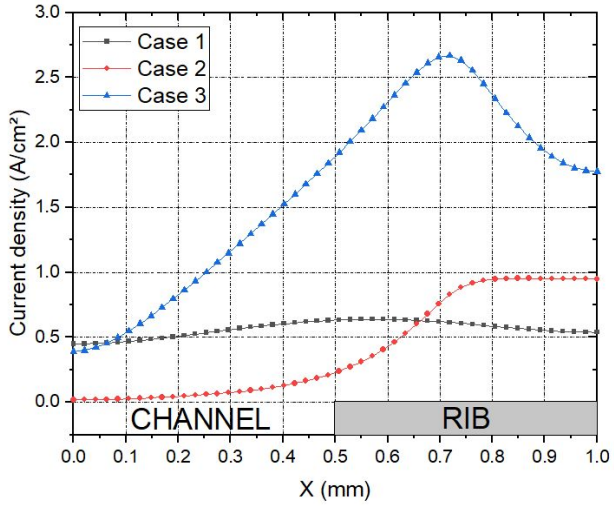

(b)

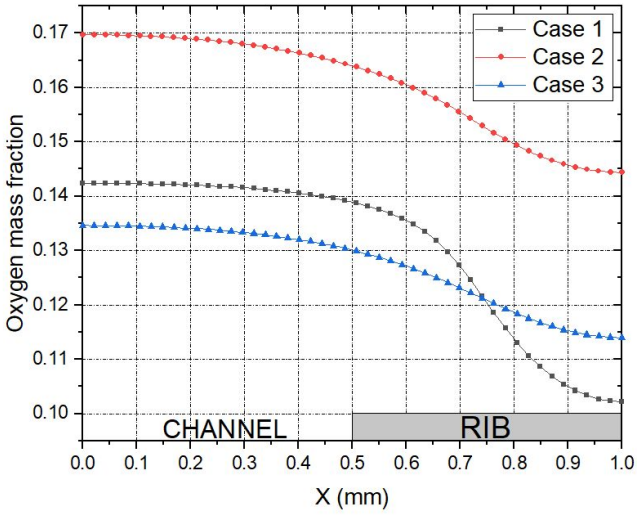

(c)

Figure 4 (a) The polarisation curves, (b) the distribution of current density within the cathode GDL at 0.55 V and (c) the distribution of oxygen mass fraction within the cathode GDL at 0.55 V for the investigated cases: Case 1 (where the GDL transport properties are anisotropic), Case 2 (where the GDL transport properties are isotropic and having the same values as those of the through-plane direction) and Case 3 (where the GDL transport properties are isotropic and having the same values as those of the in-plane direction).

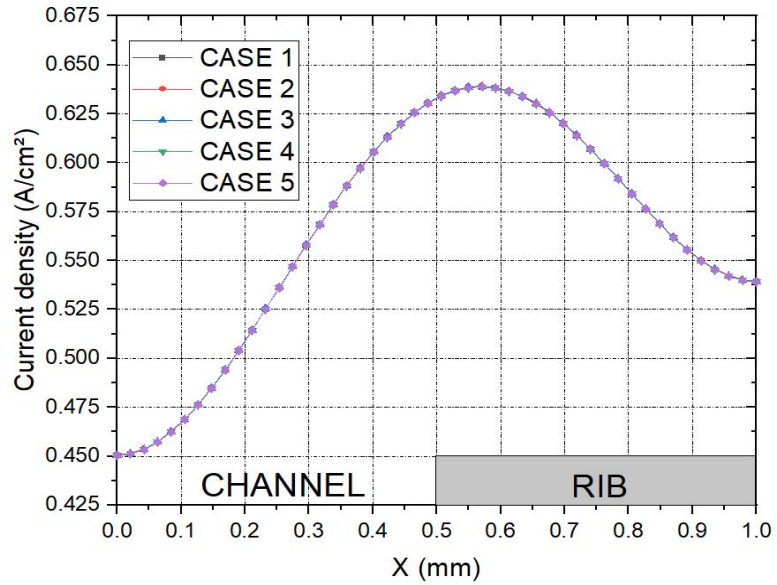

(a)

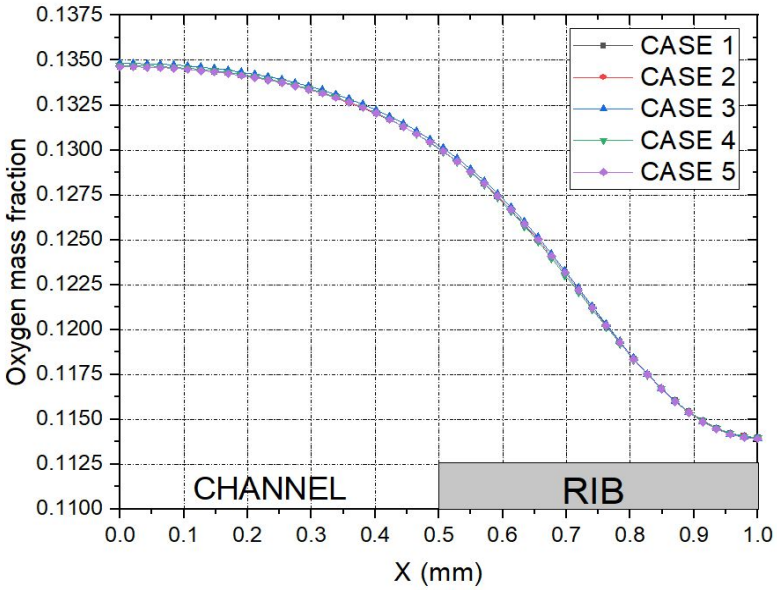

(b)

Figure 5 The distribution of (a) current density and (b) oxygen mass fraction within the cathode GDL at 0.55 V for the GDL gas permeability computation cases shown in Table 3.

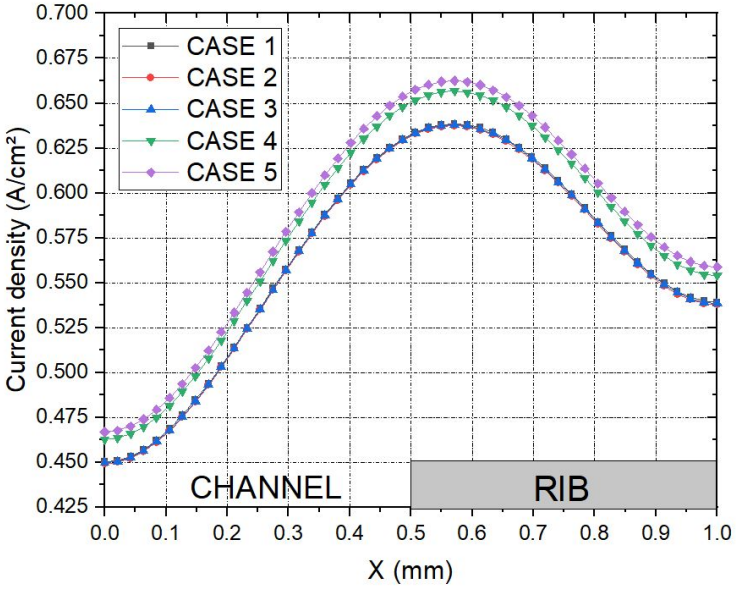

(a)

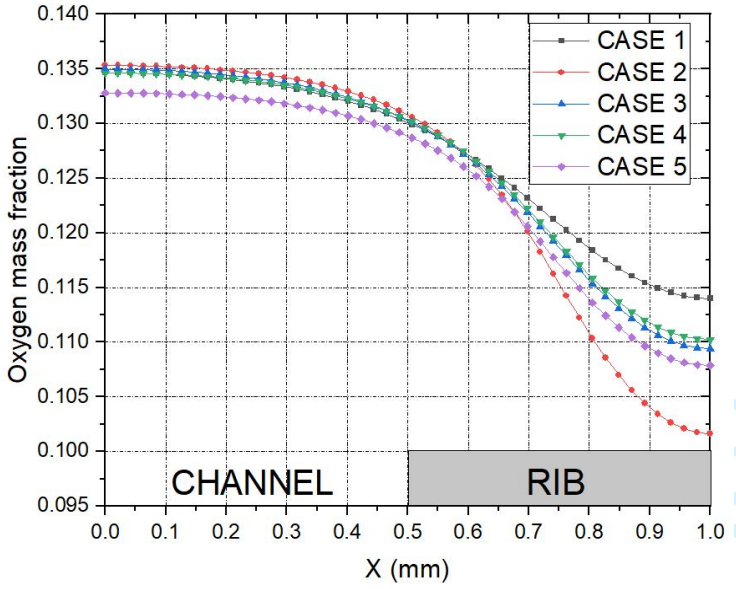

(b)

Figure 6 The distribution of (a) current density and (b) oxygen mass fraction within the cathode GDL at 0.55 V for the GDL gas diffusivity computation cases shown in Table 4.

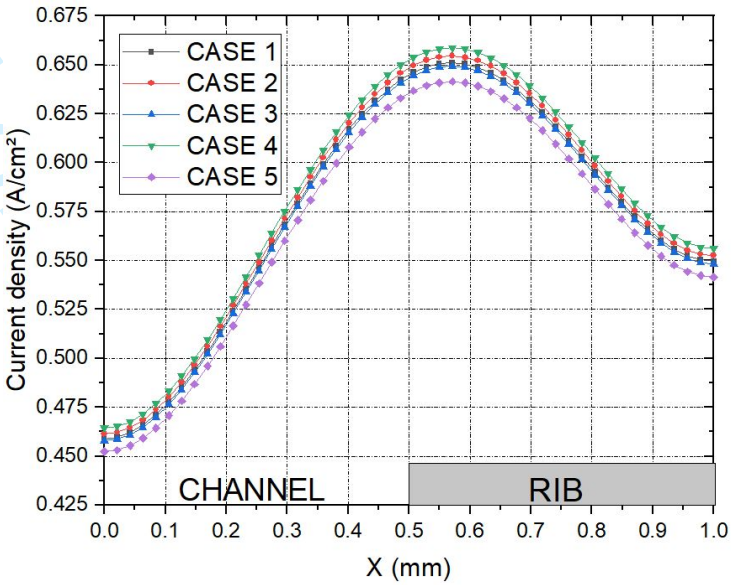

(a)

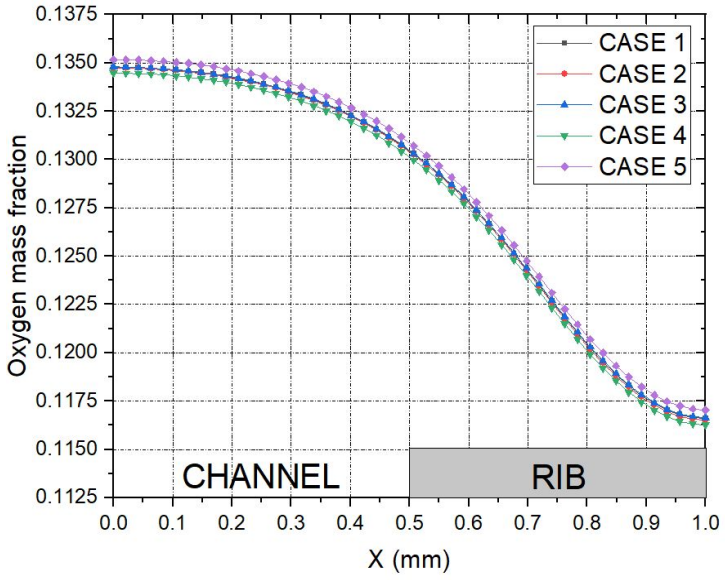

(b)

Figure 7 The distribution of (a) current density and (b) oxygen mass fraction within the cathode GDL at 0.55 V for the GDL thermal conductivity computation cases shown in Table 5.

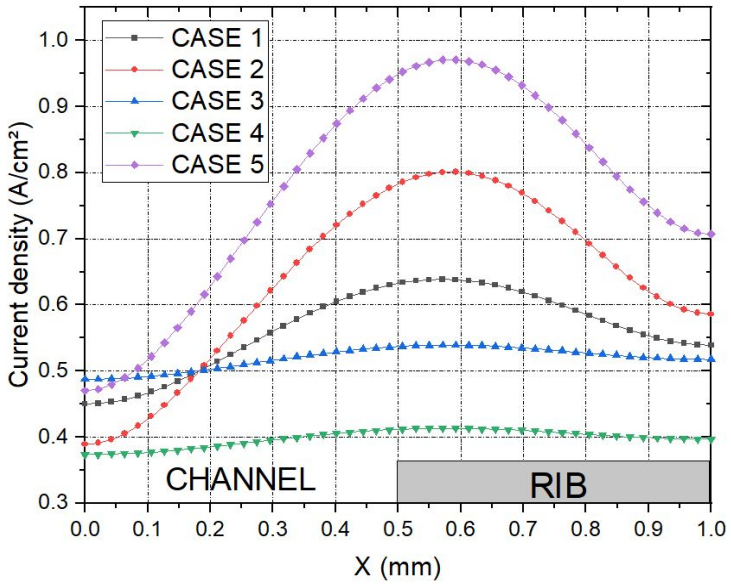

(a)

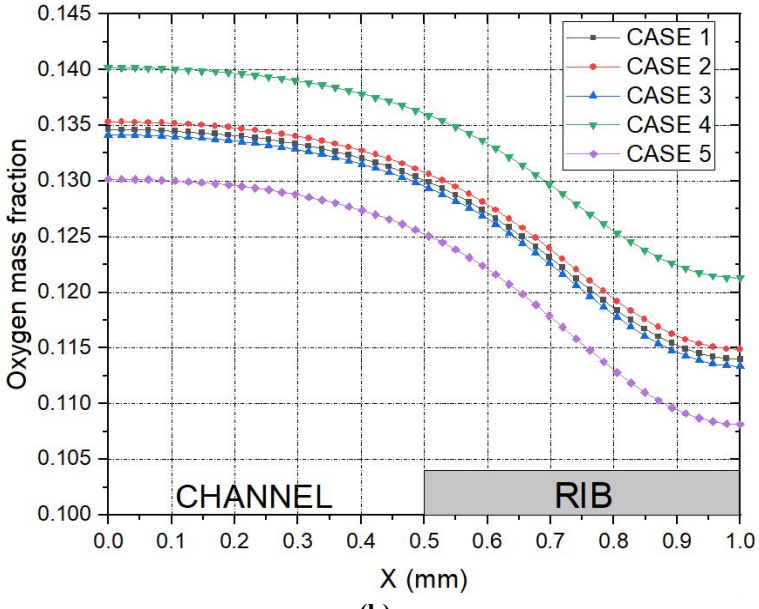

(b)

Figure 8 The distribution of (a) current density and (b) oxygen mass fraction within the cathode GDL at 0.55 V for the GDL electrical conductivity computation cases shown in Table 6.